Available online at www.sciencedirect.com
ScienceDirect
Journal of Sound and Vibration 314 (2008) 885–906
JOURNAL OF SOUND AND VIBRATION
www.elsevier.com/locate/jsvi

Modal parameter identification of mistuned bladed disks using tip timing data

Bendali Salhi[a], Joseph Lardiès[a,*], Marc Berthillier[a], Philippe Voinis[b], Charles Bodel[b]

[a]*Dept. LMARC UMR/CNRS 6174, Institut FEMTO-ST, 24, rue de l'Épitaphe, 25000 Besançon, France*
[b]*Électricité de France, Département Recherche et Développement, 92141 Clamart, France*

Received 3 October 2007; received in revised form 20 December 2007; accepted 16 January 2008
Handling Editor: C. Morfey
Available online 2 April 2008

Abstract

Two methods for the identification of the vibration characteristics of rotating engine blades from time response measurements are presented. The time responses are obtained from a mathematical blade tip timing simulation which is developed using a multi-degree-of-freedom model including structural properties of the bladed disk assembly, blade mistuning effects and aeroelastic terms. The modal parameters are identified from two subspace algorithms. The first subspace algorithm uses the properties of the shifted observability matrix. The second subspace algorithm optimizes the mutual information between the future data vector of observations and the innovation state vector. The results from the methods are compared in order to determine which of the methods is more suitable in modal parameter identification of rotating engine blades.

1. Introduction

This paper presents a contribution to the analysis of rotating machines. In particular, we are interested in the modal parameter identification of rotating engine blades using non-contact measurements. Bladed assemblies such as turbines are subjected to several sources of excitation leading to forced vibration responses that may occur at or near a blade's natural frequencies. Severe vibratory loads may cause cracks, blade failures and finally the total failure of the engine. Therefore, monitoring blade vibrations is of great importance. It prevents damage and it is possible to predict the durability and the life of blades under operating conditions. For this purpose, most engine and industrial turbine manufacturers develop measuring techniques that use several sensors in the casing around the rotor to measure and analyse the time of arrival of the blade tips at the sensors. Two standard measuring methods are used to obtain blade vibrations: the first method requires the installation of gages on some of the blades and the second method uses a frequency-modulated grid system. In the first method the measurement of rotating blade responses is performed by means of blade-mounted strain gauges. This is a very expensive contact process requiring slip ring systems and high-quality telemetry.

*Corresponding author.
E-mail address: joseph.lardies@univ-fcomte.fr (J. Lardiès).

0022-460X/$ - see front matter © 2008 Elsevier Ltd. All rights reserved.
doi:10.1016/j.jsv.2008.01.050

Furthermore, the blade-mounted strain gauges have a limited operating life as they are subjected to the harsh on-engine conditions. For the second standard method, the frequency-modulated grid method (FM grid method), permanent magnets are fitted on the tips of some blades and a specially formed wire is installed in the compressor casing above the magnets. As a blade passes a wire, the magnet produces an alternative current (AC) in the wire. Blade vibrations are interpreted from the voltage modulation of this AC signal. In this method, no signal transmitter between the rotor and the stator is needed, but the wire requires a special casing and the number of blades monitored at a time is limited to three per rotor stage. An alternative method to the two standard measuring methods is the blade tip timing (BTT) or non-intrusive stress measurement which is based on optical, capacitive or magnetic probe technology. The basic concept of this technique has been developed in Refs. [1–5]. Tip timing is a non-contacting measurement technique which uses casing mounted probes to determine the vibration of all blades. Several probes are installed in the engine casing above the rotor, and the blade transit times between the probes are measured. Fig. 1 summarizes the basic principle of this technique. Two sensors are placed around the blades. They measure the passage time of each blade in front of the sensors. The angle between these two sensors is 180°. A third sensor is placed in the proximity of the engine shaft. It measures the once-per-revolution signal. When there are no blade vibrations, the blade transit times are a function of rotor speed, rotor radius and circumferential probe position. In the case of blade vibrations, the blade transit times deviate from those obtained in the undisturbed condition, with the blades passing the probes earlier or later than normal, depending on their instantaneous deflection. The typical elements of a tip timing vibration measurement system are: the acquisition of raw arrival time data by a number of probes mounted in the casing, the derivation of blades' displacements from the measured data and the analysis of the modal parameters which describe the vibration properties of rotating bladed assemblies. Compared with the two standard methods cited previously, this technique provides notable advantages: it is non-contacting, it senses all blades and it reduces costs because it eliminates the need for rotor instrumentation and telemetry for signal transmission. This technique, however, has some drawbacks. One such drawbacks is that the measurement sampling frequency is completely dependent on the rotor speed and the number of measurement probes installed.

Methods for analysing blade tip timing data have been developed since 1970. However, given a limited number of probes, there are still no standard approaches that can identify synchronous response resonance frequencies with adequate precision. Let us recall that a synchronous response occurs when a blade's vibration frequency is an integer multiple of the engine rotation speed and an asynchronous response occurs when the

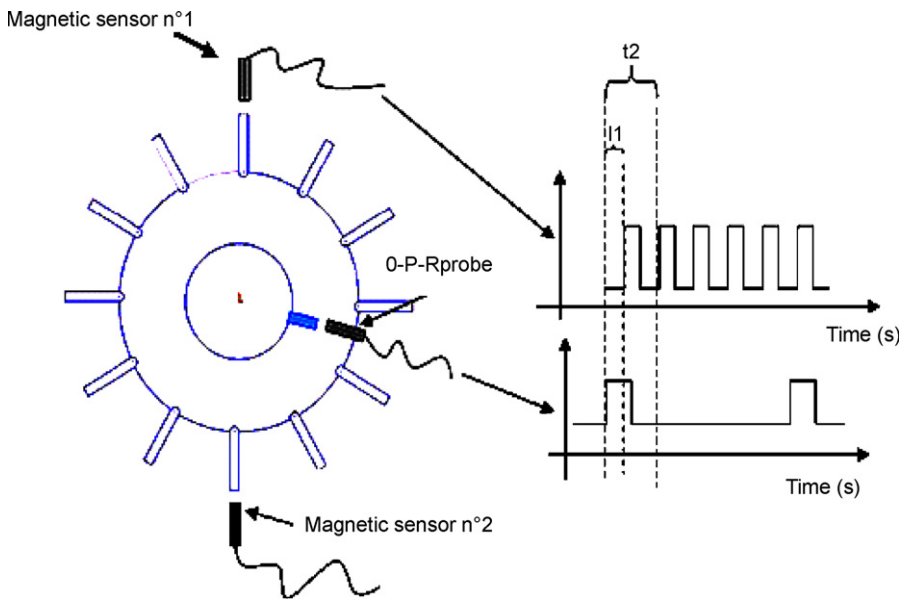

Fig. 1. A simple blade tip timing system.

blades' frequency response is a non-integer multiple of the assembly rotation speed. Synchronous vibration can be caused by mechanical effects such as residual unbalance of the rotors and non-concentric casing, as well as aerodynamic effects such as irregular pressure distributions within the airflow due to the engine intake geometry and wakes produced by upstream stators. Asynchronous vibrations are typically caused by flutter instabilities, rotating stall or by acoustic resonance. From an experimental point of view, the problem is that it is impossible to know with enough accuracy which blade will produce the largest vibration amplitude. As rotating instrumentation is limited, a challenge for the monitoring of bladed assemblies such as turbines is the use of blade tip timing methods and the analysis of BTT data can be performed either on-line or off-line. On-line data analysis provides near-real-time information updated at least once per second, while off-line analysis can provide more detailed information on individual blades, inter-blade excitations and assembly mistuning effects. The work presented in this paper concerns off-line analysis.

Carrington et al. [1] formulated three vibration analysis methods: a determinant method using four probes, a global autoregressive method and an autoregressive method with instrumental variables. They applied these methods to the tip timing problem using data obtained from a simple mathematical blade tip timing simulation. The results from the methods were compared statistically in order to determine which of the techniques is more suitable. However, all of the techniques produced biased results. In Ref. [2] Dimitriadis et al. studied the blade mistuning, the multiple engine order excitation, the combined asynchronous and synchronous resonances and the transient components in the performances of BTT data analysis. They used a simple autoregressive approach and found that major problems occur in regions where two different blade modes respond in resonance at different engine orders simultaneously.

This paper describes the use of subspace modelling for identification of blade vibration eigenfrequencies and their damping ratios using blade tip timing data. This method is applied to a lumped parameter model which produces synchronous responses. The mode shapes of the bladed assembly are also identified. This paper is organized as follows: a mathematical model of the vibrating system is given in Section 2. From this model we obtain the blade tip timing data used for the identification of modal parameters. In Section 3 we describe a method used to find the signal vibration of each blade starting from tip timing measurements. In Section 4 a signal reconstruction method is proposed to solve the aliasing problem. In Section 5 the discrete time state-space model is derived with the transition matrix which contains all modal information. In Section 6 the transition matrix is obtained by shifting properties of the observability matrix. In Section 7 the transition matrix is obtained by optimization of the mutual information criterion between the future data vector of observations and the innovation state vector. The effectiveness of these two methods is presented and discussed in Section 8 where numerical results are presented. This paper is briefly concluded in Section 9.

2. Vibration analysis of the simulated model

The blade tip timing data analysis methods developed in this paper are applied to simulated time data obtained from a mathematical model of the forced response of a rotating bladed assembly. Fig. 2 shows the basic layout of the mechanical model. For illustrative purposes only three blades represented by a mass–spring–damper system are shown in this figure and it is assumed that each blade in the assembly has one significant mode which is the first bending. This system has blade degrees-of-freedom (dof) and disk (dof) for

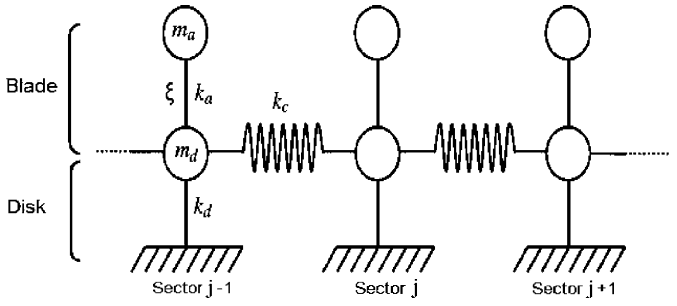

Fig. 2. Two degrees of freedom per sector model.

each sector. Each disk is coupled to neighbouring sectors by springs of stiffness k_c. A structural damping, whose damping ratio is ξ, is shown in the model. This model simulates the dynamic behaviour of a blade assembly which has twenty two blades, and provides a temporal forced response of each blade. The main objective of the sweeping simulator is to attempt to produce data similar to the experimental blade tip timing data obtained from tests on fans, turbines and other bladed assemblies. Random excitations are generated to obtain the forced responses of the system and only steady-state responses are considered for the identification of modal parameters. This model will provide the temporal forced response of each blade. The equations of motion for this model are

$$\mathbf{M}_0\ddot{\mathbf{q}}(t) + \mathbf{C}_0\dot{\mathbf{q}}(t) + \mathbf{K}_0\mathbf{q}(t) = \mathbf{F}_{\text{aero}}(t) + \mathbf{F}_{\text{turb}}(t) \tag{1}$$

where $\mathbf{q}(t)$ is the vector of displacements corresponding to (2×22) dofs. The displacement in sector j is given by

$$\mathbf{q}^j(t) = \begin{bmatrix} \mathbf{q}_1^j(t) \\ \mathbf{q}_2^j(t) \end{bmatrix} \tag{2}$$

the subscript 1 represents the blade and the subscript 2 represents the disk. In fact, the displacement for all sectors is given by the global (44×1) vector

$$\mathbf{q}(t) = \begin{bmatrix} \mathbf{q}^1(t) \\ \vdots \\ \mathbf{q}^{44}(t) \end{bmatrix}. \tag{3}$$

$\mathbf{M}_0$, $\mathbf{C}_0$ and $\mathbf{K}_0$ represent the structural mass, damping and stiffness matrices of dimension $(n' \times n')$ with $n' = 44$. The mass matrix $\mathbf{M}_0$ is given by

$$\mathbf{M}_0 = \begin{bmatrix} \mathbf{M}_s & 0 & \cdots & 0 \\ 0 & \mathbf{M}_s & \cdots & 0 \\ \vdots & \vdots & \vdots & \vdots \\ 0 & 0 & \cdots & \mathbf{M}_s \end{bmatrix} \quad \text{with } \mathbf{M}_s = \begin{bmatrix} m_a & 0 \\ 0 & m_d \end{bmatrix} \tag{4}$$

where m_a is a modal mass of blade j and m_d is a modal mass of a part of disk j.

The stiffness matrix $\mathbf{K}_0$ is given by

$$\mathbf{K}_0 = \begin{bmatrix} \mathbf{K}^a & \mathbf{K}^b & 0 & \cdots & \mathbf{K}^b \\ \mathbf{K}^b & \mathbf{K}^a & \mathbf{K}^b & \cdots & 0 \\ 0 & \mathbf{K}^b & \mathbf{K}^a & \cdots & 0 \\ \vdots & \vdots & \vdots & \vdots & \vdots \\ \mathbf{K}^b & 0 & \cdots & \mathbf{K}^b & \mathbf{K}^a \end{bmatrix} \tag{5}$$

with

$$\mathbf{K}^a = \begin{bmatrix} k_a & -k_a \\ -k_a & k_a + k_d + 2k_c \end{bmatrix} \tag{6}$$

and

$$\mathbf{K}^b = \begin{bmatrix} 0 & 0 \\ 0 & -k_c \end{bmatrix}. \tag{7}$$

The damping matrix is given by

$$\mathbf{C}_0 = \mathbf{P}^{-\mathrm{T}}\mathrm{Diag}(4\pi f_i \xi_i)\mathbf{P}^{-1} \tag{8}$$

where f_i is the ith natural frequency, ξ_i is the ith damping ratio and $\mathbf{P}$ is the matrix containing the conservative mode shapes. An aeroelastic force $\mathbf{F}_{\text{aero}}(t)$ has been introduced into the model, by way of circulant matrix coefficients, considering only five different coefficients (see Ref. [6] and Appendix A). This force is a function of displacement $\mathbf{q}(t)$ and velocity $\dot{\mathbf{q}}(t)$:

$$\mathbf{F}_{\text{aero}}(t) = \mathbf{C}^R_{\text{aero}}\dot{\mathbf{q}}(t) - \omega\mathbf{C}^I_{\text{aero}}\mathbf{q}(t) \tag{9}$$

where $\mathbf{C}^R_{\text{aero}}$ and $\mathbf{C}^I_{\text{aero}}$ are two (44×44) matrices containing the aeroelastic coefficients, C_0, C_1, C_{-1}, C_2 and C_{-2}, which have been computed with a software developed by our research group (EDF R& D). These two matrices are given in Appendix A. The angular excitation frequency is given by ω. A white noise excitation simulates the turbulence excitation $\mathbf{F}_{\text{turb}}(t)$ and generates the time-forced response. It is representative of turbulent excitation of the blades by the fluid. Eq. (1) becomes

$$\mathbf{M}_0\ddot{\mathbf{q}}(t) + \mathbf{C}_{\text{damp}}\dot{\mathbf{q}}(t) + \mathbf{K}_{\text{stiff}}\mathbf{q}(t) = \mathbf{F}_{\text{turb}}(t) \tag{10}$$

where $\mathbf{K}_{\text{stiff}}$ and $\mathbf{C}_{\text{damp}}$ are given by the following formula (see Appendix A):

$$\mathbf{K}_{\text{stiff}} = \mathbf{K}_0 + \omega\mathbf{C}^I_{\text{aero}} \tag{11}$$

and

$$\mathbf{C}_{\text{damp}} = \mathbf{C}_0 - \mathbf{C}^R_{\text{aero}}. \tag{12}$$

The stiffness coefficients have been chosen so that the blade modes are well separated from the disk modes: the blade mode family has frequencies around 60 Hz and the lowest frequency for a disk mode is close to 500 Hz. Turbo machinery blade rows are designed to contain identical blades, identically mounted, and uniformly spaced on the disk within a given blade row. When this is satisfied, the blade row is called tuned. However, minor differences in structural and material properties and in blade attachments are inherently present among the blades. These variations arise because of manufacturing tolerances, variations in material properties, small imperfections, wear and tear and other similar factors. Bladed disks are only quasi-cyclic structures. As a consequence, the dynamic behaviour of actual bladed disks may be drastically modified in comparison with their cyclic idealization. The variations in blade properties and the flow field from one blade to another are referred to as mistuning. In the case of mistuned blades the vibration energy of the system is concentrated in a few blades, and these blades have important amplitudes. A higher response amplitude implies a higher level of stress in the blade and so the stresses in a mistuned blade row will be higher than the stresses present in a tuned blade row. A significant risk of fatigue failure will exist because of the presence of mistuning. Hence, it is essential to understand the effects of mistuning on the designed bladed disk. Mistuning is modelled by adding stiffness variations to nominal blade stiffness. Mistuning is defined by the presence of small blade-to-blade variations of their structural and (or) geometrical properties, which may produce large increases in the forced response of some of the blades. The ith mistuned stiffness is expressed as

$$k_{a,i} = k_a(1 + \delta_i) \quad \text{with } i = 1, 2, \ldots, 22 \tag{13}$$

where δ_i is the ith mistuning value which is given randomly or intentionally. It is assumed that each blade in the assembly has one significant mode: the first bending mode. The eigenvalues of the transition matrix of the vibrating system contain the eigenfrequencies and the damping coefficients of the tuned and mistuned model and are presented in Fig. 3. We can see that the tuned system is unstable and that the mistuned model system is stable. Mistuning couples all the tuned modes and stabilizes the unstable modes. These computed eigensolutions are called exact solutions and our objective is to compare these exact modal parameters to identified modal parameters obtained by subspace algorithms developed in the paper. Fig. 4 presents tuned and mistuned mode shapes. It is shown from these figures that the mode shapes of bladed assemblies are influenced by the mistuning. The mistuned mode shapes present a localization of the vibration energy on certain blades and this phenomenon has a dangerous consequence for the structure behaviour.

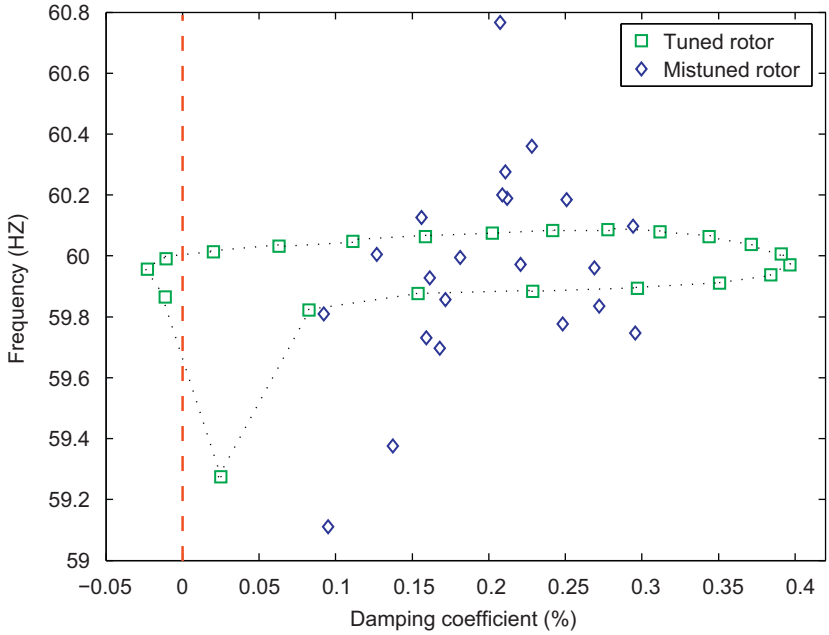

Fig. 3. Stability loop for the tuned and mistuned models.

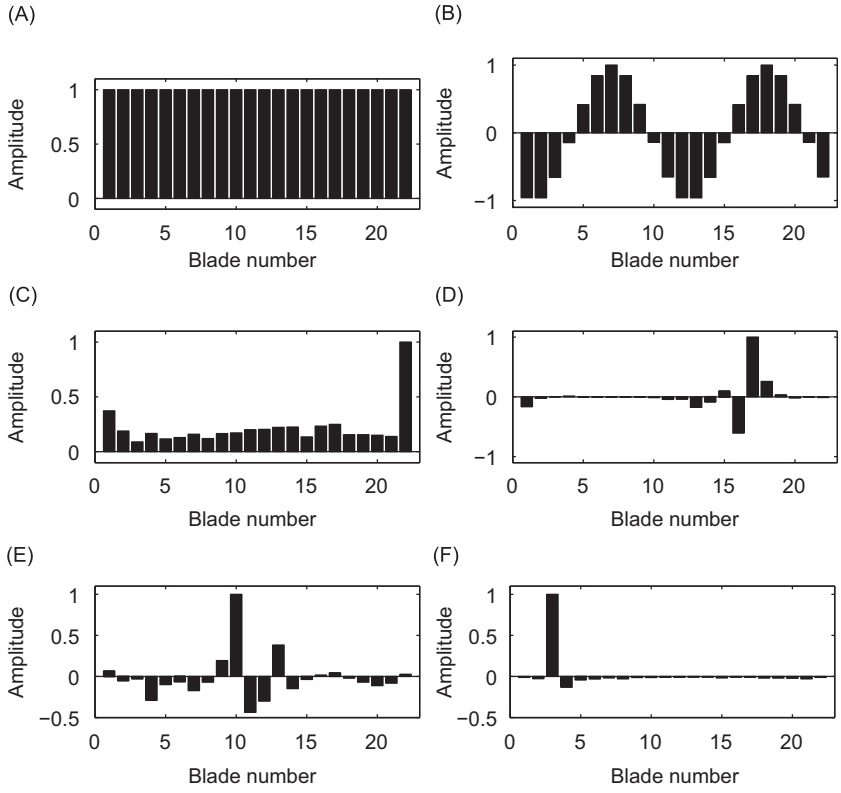

Fig. 4. Comparison between tuned and mistuned mode shapes: (A) tuned mode shape with 0 diameter; (B) tuned mode shape with 2 diameter; (C) first mistuned mode shape; (D) mistuned mode shape number 6; (E) mistuned mode shape number 10; (F) mistuned mode shape number 22.

3. Analysis of tip timing measurements

Tip timing methods are used to measure bladed assembly vibrations. The BTT method relies on a number of probes placed around the casing of the engine and detecting each blade tip as it passes in front of the probes. The time of arrival of the blades at each probe is compared to the times at which the blades would have arrived without vibration. The difference between the two times yields the displacements of the blade tips when passing the relevant probe at each revolution. The analysis of the difference in time allows us to find the vibratory displacement of each blade. The measured time is given by the following formula:

$$t_k = t_0 + \delta t \tag{14}$$

where t_k is the time of arrival of the blade k, t_0 is the time of arrival once per revolution and δt is the variations of time of arrival.

From δt we find the vibratory displacement of the blade k at time t_k using the following relation:

$$d(t_k) = -R\Omega_r \delta t(t_k) \tag{15}$$

where R is the external ray of the bladed assemblies and Ω_r is the assembly rotational speed.

The response signal for each blade in the assembly can be analysed individually using standard Fourier transform; however, from the sampling theory, the frequency components of the assembly response are defined up to the frequency, $\omega_{\max}$, given by the following relation:

$$\omega_{\max} = \frac{\Omega_r M}{2} \tag{16}$$

where M is the number of response measurement points around the periphery (or the number of probes). Only response components with a frequency less than half the rotation rate are defined uniquely. All other frequency components are present as artefacts in the measured signal. This type of signal distorsion is called aliasing. The probe measurements are discrete pulses that occur once per revolution and from the under-sampling of BTT signals we reconstruct a continuous signal of displacements.

4. Reconstruction of the signal

The subspace method requires signals without aliasing and a regular sampling of these signals to identify modal parameters, whereas the tip timing method gives signals with aliasing and under-sampling signals. Under-sampling of BTT signals cannot be taken into account in the subspace method. To solve this problem and find a link between the subspace method and tip timing data, an interpolation technique is proposed in this paragraph. In fact, under-sampled signals are used to reconstruct a continuous signal using the Shannon sampling theorem. This theorem is given by the following expression [7]:

$$s(t) = \sum_{k=-\infty}^{+\infty} s_{\mathrm{AC}}\left(\frac{k}{v_s}\right) \frac{\sin(v_s t - k)}{(v_s t - k)} \tag{17}$$

where k is the number of samples and s_{AC} is the complex signal of the real signal s_a (signal with aliasing) given by the tip timing analysis method. The Hilbert transform is used to compute s_{AC} from s_a.

Let s_{AR} be the interpolated signal of bandwidth B and centre frequency f_0. Its expression is given by the following relation:

$$s_{\mathrm{AR}}(t) = \mathrm{Re}(s(t)\exp(i2\pi f_0 t)). \tag{18}$$

An analytic band-pass signal with bandwidth B and centre frequency f_0 can be perfectly reconstructed from samples of the corresponding complex envelope at a sub-sampling rate $v_s > B$. Hence, the sampling rate v_s can be much smaller than twice the highest frequency $(f_0 + B/2)$. The following formula describes the reconstruction of this signal:

$$s_{\mathrm{AR}}(t) = \mathrm{Re}\left[\sum_{k=-\infty}^{+\infty} s_{\mathrm{AC}}\left(\frac{k}{v_s}\right) \frac{\sin(v_s t - k)}{(v_s t - k)} \exp(i2\pi(f_0/v_s)(v_s t - k))\right]. \tag{19}$$

Using this formula, the original high-frequency signals s_{AR} can be reconstructed at an arbitrary time sample, which is important for many applications, such as tip timing measurements. However, formulas of this type are known to be impractical, since the $\sin(x)/x$ function decays very slowly, so that many terms of the series have to be evaluated for accurate reconstruction. A well-known approach to avoid this problem in the complex envelope or low-pass case is to use reconstruction kernels K that are time limited so that only a finite number of samples have to be considered. The general reconstruction formula given by Ries [7], for s_{AR} sampled at rate v_s, is

$$K_{v_s} s_{AR}(t) = \mathrm{Re}\left[\sum_{k=-\infty}^{+\infty} s_{AC}\left(\frac{k}{v_s}\right) K(v_s t - k) \exp(i2\pi(f_0/v_s)(v_s t - k))\right] \tag{20}$$

where K is a piecewise continuous function. The optimum kernel for an arbitrary order p is given in the time domain by

$$K_{\mathrm{optimum}}(t) = \sum_{l=0}^{[(p-l)/2]} (-1)^l b_{lp} D^{2l} B_p(t) \tag{21}$$

where B_p is the B-spline function of order p. It is a piecewise polynomial of degree $p-1$ with finite support in $[-p/2, p/2]$, defined recursively by

$$B_p(t) = \frac{1}{(p-1)!} \sum_{k=0}^{[p/2-t]} (-1)^k \binom{p}{k} \left(\frac{p}{2} - |t| - k\right)^{(p-1)} \tag{22}$$

$$t \in [-p/2, p/2]$$

and

$$B_p(t) = (B_{p-1} * B_1)(t) \tag{23}$$

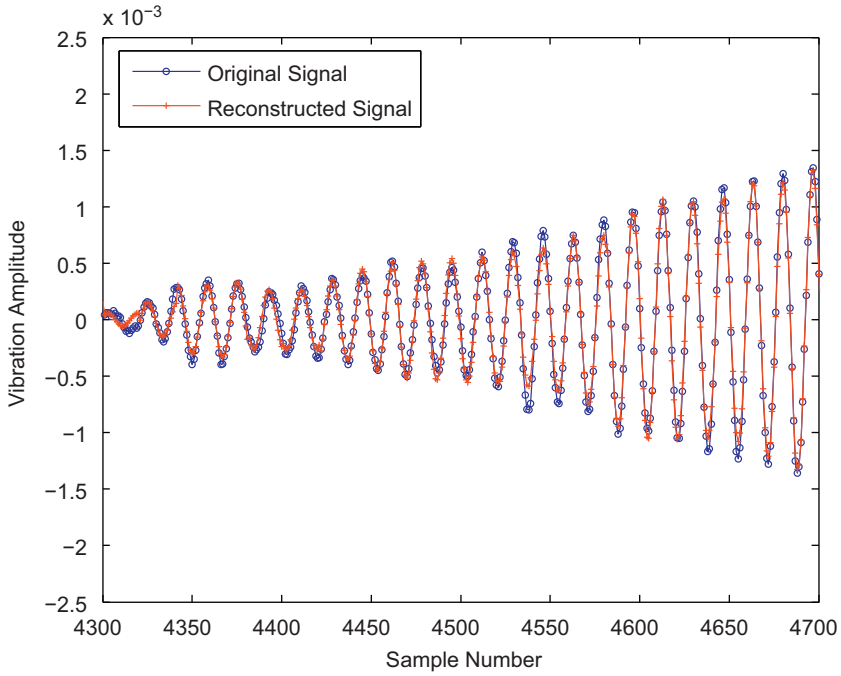

Fig. 5. Reconstruction of the signal.

is the p-fold convolution of the rect-function, which is equal to B_1, with itself. The number b_{lp} is defined by

$$\left(\frac{t/2}{\sin(t/2)}\right)^p = \sum_{l=0}^{\infty} b_{lp} t^{2l}. \tag{24}$$

Fig. 5 presents the results obtained using the reconstruction formula (20). In this figure the reconstructed signal (obtained from the signal with aliasing) is compared to the original signal (the same signal computed without aliasing). Reconstruction error is given by the 2-*norm* difference between the reconstructed and the original signal. For $p = 1$ the error of reconstruction is equal to $6 \cdot 10^{-3}$.

5. The discrete state-space representation

Let m be the number of analysed blades ($r \leqslant m$). To Eq. (10) the $(m \times 1)$ observation equation is added

$$\mathbf{y}(t) = \mathbf{L}\mathbf{q}(t) + \mathbf{v}(t) \tag{25}$$

where $\mathbf{L}$ is the $(m \times n')$ output influence matrix for the displacement, describing the relationship between the vector $\mathbf{q}(t)$ and the measurement vector $\mathbf{y}(t)$ and $\mathbf{v}(t)$ is an $(m \times 1)$ additive noise disturbance, a vector of measurement errors simulated by a gaussian white noise. The modal characteristics (μ , $\mathbf{\Psi}_\mu$) of the vibrating system are solutions of

$$\det(\mathbf{M}_0\mu^2 + \mathbf{C}_{\text{damp}}\mu + \mathbf{K}_{\text{stiff}}) = 0 \tag{26}$$

and

$$(\mathbf{M}_0\mu^2 + \mathbf{C}_{\text{damp}}\mu + \mathbf{K}_{\text{stiff}})\mathbf{\Psi}_\mu = 0 \tag{27}$$

where det(.) represents a determinant. The system described by Eqs. (10) and (25) is equivalent to the following continuous time state-space model [8–10]:

$$\dot{\mathbf{x}}(t) = \tilde{\mathbf{A}}x(t) + \tilde{\mathbf{B}}\boldsymbol{\eta}(t) \tag{28}$$

$$\mathbf{y}(t) = \mathbf{C}x(t) + \mathbf{v}(t) \tag{29}$$

where $\mathbf{x}(t)$ is the state vector of dimension $n = 2n'$

$$\mathbf{x}(t) = \begin{bmatrix} \mathbf{q}(t) \\ \dot{\mathbf{q}}(t) \end{bmatrix}. \tag{30}$$

$\tilde{\mathbf{A}}$ is an n by n state matrix, $\tilde{\mathbf{B}}$ is an n by n' matrix containing the bloc matrix $\mathbf{M}_0^{-1}$ and $\mathbf{C}$ is an m by n output influence matrix including displacement only:

$$\tilde{\mathbf{A}} = \begin{bmatrix} \mathbf{0} & \mathbf{I} \\ -\mathbf{M}_0^{-1}\mathbf{K}_{\text{stiff}} & -\mathbf{M}_0^{-1}\mathbf{C}_{\text{damp}} \end{bmatrix} \tag{31}$$

and

$$\tilde{\mathbf{B}} = \begin{bmatrix} \mathbf{0} \\ \mathbf{M}_0^{-1} \end{bmatrix}; \quad \mathbf{C} = [\mathbf{L}\ \ \mathbf{0}]. \tag{32}$$

Eqs. (28) and (29) constitute a continuous time state-space model of the dynamical system and the order of the system is the dimension of the state matrix. Given the initial condition $\mathbf{x}(t_0)$ at some $t = t_0$ and solving for $\mathbf{x}(t)$ from Eq. (28) yields

$$\mathbf{x}(t) = \mathrm{e}^{\tilde{\mathbf{A}}(t-t_0)}\mathbf{x}(t_0) + \int_{t_0}^{t} \mathrm{e}^{\tilde{\mathbf{A}}(t-\tau)}\tilde{\mathbf{B}}\mathbf{F}_{\text{turb}}(\tau)\,\mathrm{d}\tau. \tag{33}$$

This equation describes the variation with time of the state variable $\mathbf{x}(t)$ with respect to the initial condition $\mathbf{x}(t_0)$ and the input $\mathbf{F}_{\text{turb}}(t)$. The evaluation of $\mathbf{x}(t)$ at equally spaced intervals of time t can be obtained by a

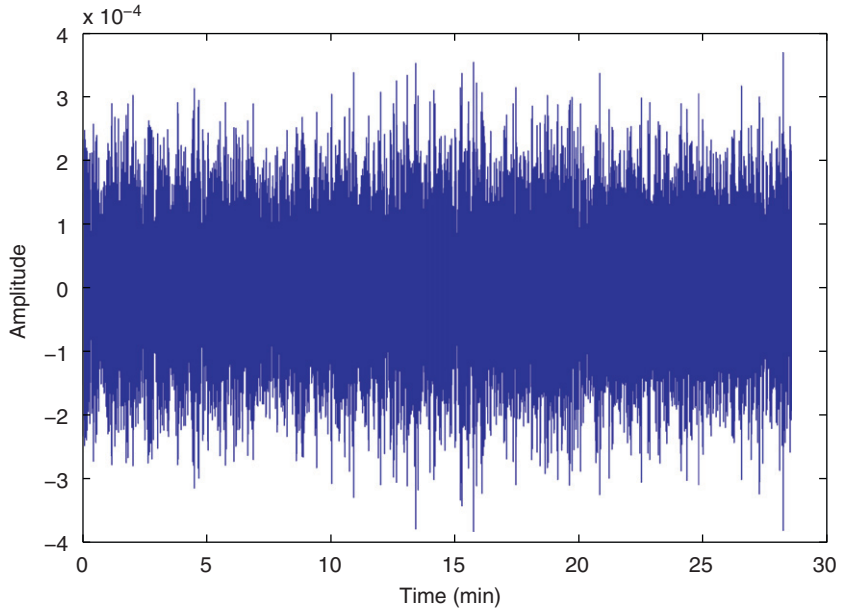

Fig. 6. A typical temporal response obtained from a blade.

discrete time representation of Eq. (33). Let the equally spaced times be given by $0, \Delta t, 2\Delta t, \ldots, (k+1)\Delta t, \ldots$ where Δt is a constant sampling period. Consider $t = (k+1)\Delta t$ and $t_0 = k\Delta t$; Eq. (33) becomes

$$\mathbf{x}[(k+1)\Delta(t)] = \mathrm{e}^{\tilde{\mathbf{A}}\Delta t}\mathbf{x}(k\Delta t) + \int_{k\Delta t}^{(k+1)\Delta t} \mathrm{e}^{\tilde{\mathbf{A}}[(k+1)\Delta t-\tau]}\tilde{\mathbf{B}}\mathbf{F}_{\mathrm{turb}}(\tau)\,\mathrm{d}\tau. \tag{34}$$

The $(n \times n)$ discrete time state-space matrix or discrete time transition matrix is defined by the following relation:

$$\mathbf{A} = \mathrm{e}^{\tilde{\mathbf{A}}\Delta t} \tag{35}$$

$\mathbf{x}_{k+1} = \mathbf{x}[(k+1)\Delta t]$ is the discrete time state vector and $\mathbf{u}_k = \int_{k\Delta t}^{(k+1)\Delta t} \mathrm{e}^{\tilde{\mathbf{A}}[(k+1)\Delta t-\tau]}\tilde{\mathbf{B}}\mathbf{F}_{\mathrm{turb}}(\tau)\,\mathrm{d}\tau$ is the global input vector.

The discrete time state-space model is given by the following formula:

$$\mathbf{x}_{k+1} = \mathbf{A}\mathbf{x}_k + \mathbf{u}_k \tag{36}$$

and the discrete time observation equation or output observation vector is given by the following expression:

$$\mathbf{y}_k = \mathbf{C}\mathbf{x}_k + \mathbf{v}_k. \tag{37}$$

The time responses of 22 blades are used in the identification process and the two previous discrete equations form the basis of the system identification procedure. Fig. 6 shows a part of the time response of a blade used in the identification process.

6. Identification of modal parameters by shifting the observability matrix

The eigenvalues λ_i and eigenvectors Φ_{λ_i} of the discrete time transition matrix $\mathbf{A}$ are related to the modal characteristics [8–10] by

$$\lambda_i = \mathrm{e}^{\mu_i \Delta t} \quad \text{and} \quad \mathbf{C}\Phi_{\lambda_i} = \mathbf{L}\Psi_{\lambda_i}. \tag{38}$$

The global modal parameters: the natural frequencies f_i and damping ratios ξ_i of the vibrating system can be determined by (demonstration is given in Appendix B)

$$f_i = \frac{1}{2\pi\Delta t}\sqrt{[\ln(\lambda_i\lambda_i^*)]^2 + 4\left[\arccos\left(\frac{\lambda_i+\lambda_i^*}{2\sqrt{\lambda_i\lambda_i^*}}\right)\right]^2} \tag{39}$$

$$\xi_i = \sqrt{\frac{[\ln(\lambda_i\lambda_i^*)]^2}{[\ln(\lambda_i\lambda_i^*)]^2 + 4\left[\arccos\left(\frac{\lambda_i+\lambda_i^*}{2\sqrt{\lambda_i\lambda_i^*}}\right)\right]^2}} \tag{40}$$

for $i = 1, 2, \ldots, n'$.

Our objective is to obtain the discrete time transition matrix $\mathbf{A}(n \times n)$ from the output observation vector $\mathbf{y}_k(m \times 1)$.

Define $\mathbf{y}_k^+ = [\mathbf{y}_k^{\mathrm{T}}, \mathbf{y}_{k+1}^{\mathrm{T}}, \ldots, \mathbf{y}_{k+f-1}^{\mathrm{T}}]^{\mathrm{T}}$ the $(mf \times 1)$ future data vector and $\mathbf{y}_{k-1}^- = [\mathbf{y}_{k-1}^{\mathrm{T}}, \mathbf{y}_{k-2}^{\mathrm{T}}, \ldots, \mathbf{y}_{k-p}^{\mathrm{T}}]^{\mathrm{T}}$ the $(mp \times 1)$ past data vectors, where the superscript $(.)^{\mathrm{T}}$ denotes the transpose operation. The $(mf \times mp)$ covariance matrix between the future and the past is [11]

$$\mathbf{H} = E[\mathbf{y}_k^+(\mathbf{y}_{k-1}^-)^{\mathrm{T}}] = \begin{bmatrix} \mathbf{R}_1 & \mathbf{R}_2 & \cdots & \mathbf{R}_p \\ \mathbf{R}_2 & \mathbf{R}_3 & \cdots & \mathbf{R}_{p+1} \\ \vdots & \vdots & \vdots & \vdots \\ \mathbf{R}_f & \mathbf{R}_{f+1} & \cdots & \mathbf{R}_{f+p-1} \end{bmatrix} \tag{41}$$

where E denotes the expectation operator and $\mathbf{H}$ is the block Hankel matrix (a block band counter diagonal matrix) formed with the $(m \times m)$ individual auto covariance matrices $\mathbf{R}_i = E[\mathbf{y}_{k+i}\mathbf{y}_k^{\mathrm{T}}] = \mathbf{C}\mathbf{A}^{i-1}\mathbf{G}$, with $\mathbf{G} = E[\mathbf{x}_{k+1}\mathbf{y}_k^{\mathrm{T}}]$. The auto covariance matrices are estimated from T data points and computed by

$$\hat{\mathbf{R}}_i = \frac{1}{T}\sum_{k=1}^{\mathrm{T}} \mathbf{y}_{k+i}\mathbf{y}_k^{\mathrm{T}}, \quad i = 1, 2, \ldots, p+f \tag{42}$$

and with these auto covariance matrices we form the block Hankel matrix. In order to identify the transition matrix $\mathbf{A}$ and the output influence matrix $\mathbf{C}$ two matrix factorizations of $\mathbf{H}$ are employed: the QR factorization and the factorization of $\mathbf{H}$ into its observability and controllability matrices. The first factorization uses the orthogonal-triangular (QR) decomposition of $\mathbf{H}$ as $\mathbf{H} = \mathbf{QR}$, where $\mathbf{Q}$ is a unitary matrix and $\mathbf{R}$ an upper triangular matrix [12]. The second factorization of the block Hankel matrix $\mathbf{H}$ considers its $(mf \times n)$ observability and $(n \times mp)$ controllability matrices, $\mathbf{O}$ and $\mathbf{K}$, as

$$\mathbf{H} = \begin{bmatrix} \mathbf{CG} & \mathbf{CAG} & \cdots & \mathbf{CA}^{p-1}\mathbf{G} \\ \mathbf{CAG} & \mathbf{CA}^2\mathbf{G} & \cdots & \mathbf{CA}^{p}\mathbf{G} \\ \vdots & \vdots & \vdots & \vdots \\ \mathbf{CA}^{f-1}\mathbf{G} & \mathbf{CA}^{f}\mathbf{G} & \cdots & \mathbf{CA}^{f+p-2}\mathbf{G} \end{bmatrix} = \begin{bmatrix} \mathbf{C} \\ \mathbf{CA} \\ \vdots \\ \mathbf{CA}^{f-1} \end{bmatrix} [\mathbf{G}\ \ \mathbf{AG}\ \ \cdots\ \ \mathbf{A}^{p-1}\mathbf{G}] = \mathbf{OK}. \tag{43}$$

The two factorizations of the block Hankel matrix are equated to give

$$\mathbf{H} = \mathbf{QR} = \mathbf{OK}. \tag{44}$$

From this equation the observability matrix $\mathbf{O}$ is computed. To identify the transition matrix $\mathbf{A}$ we consider the following property which is deduced from the structure of the observability matrix $\mathbf{O}$.

Let $\mathbf{O}^{\downarrow}$ be the $m(f-1)\times n$ matrix obtained from $\mathbf{O}$ by deleting the last block row of $\mathbf{O}$ and let $\mathbf{O}^{\uparrow}$ be the $m(f-1)\times n$ matrix obtained from $\mathbf{O}$ by deleting the first block row of $\mathbf{O}$

$$\mathbf{O}^{\downarrow}=\begin{bmatrix}\mathbf{C}\\ \mathbf{CA}\\ \vdots\\ \mathbf{CA}^{f-2}\end{bmatrix}\quad\text{and}\quad\mathbf{O}^{\uparrow}=\begin{bmatrix}\mathbf{CA}\\ \mathbf{CA}^{2}\\ \vdots\\ \mathbf{CA}^{f-1}\end{bmatrix}. \tag{45}$$

We obtain

$$\mathbf{O}^{\downarrow}\mathbf{A}=\mathbf{O}^{\uparrow}. \tag{46}$$

The least squares estimate of $\mathbf{A}$ is then

$$\mathbf{A}=(\mathbf{O}^{\downarrow})^{+}\mathbf{O}^{\uparrow}. \tag{47}$$

The superscript + indicates a pseudo-inverse. The value of the matrix $\mathbf{C}$ is given by the first block row of the observability matrix $\mathbf{O}$

$$\mathbf{C}=\mathbf{O}_{1\mathrm{R}}=\text{the first block row of }\mathbf{O}. \tag{48}$$

Another method using an innovation representation and optimizing the mutual information between the past and future observations is presented in the next section.

7. Identification of modal parameters using an innovation representation and the mutual information criterion

Since the state vector $\mathbf{x}_k$ of dimension $n=2n'$ is not observable (only the vector of observations $\mathbf{y}_k$ is measured) we estimate it and transform Eqs. (28) and (29) into a state-space innovation form, before the discrete time transition matrix $\mathbf{A}$ and the output influence matrix $\mathbf{C}$ are computed. $\mathbf{x}_k$ is estimated by its orthogonal projection onto the subspace spanned by the stacked vector of past data vectors denoted $\mathbf{y}_{k-1}^{-}$ and the notation $\mathbf{z}_k=\mathbf{x}_k|\mathbf{y}_{k-1}^{-}$ is used to denote this orthogonal projection. Note that if a and b are two zero-mean random vectors, the orthogonal projection of a onto the manifold spanned by b is by definition

$$a|b=E[ab^{\mathrm{T}}](E[bb^{\mathrm{T}}])^{-1}b. \tag{49}$$

To obtain $\mathbf{z}_{k+1}$ advance the time index by 1 in $\mathbf{z}_k$ and use properties of the orthogonal projection defined in Ref. [11]

$$\mathbf{z}_{k+1}=\mathbf{x}_{k+1}|\mathbf{y}_k^{-}=\mathbf{x}_{k+1}|\mathbf{y}_{k-1}^{-}+\mathbf{x}_{k+1}|\mathbf{e}_k=\mathbf{A}(\mathbf{x}_k|\mathbf{y}_{k-1}^{-})+\mathbf{B}\mathbf{e}_k=\mathbf{A}\mathbf{z}_k+\mathbf{B}\mathbf{e}_k, \tag{50}$$

where $\mathbf{e}_k=\mathbf{y}_k-\mathbf{y}_k$ is called the innovation component in the data vector $\mathbf{y}_k$. It is an $(m\times 1)$ stochastic vector with zero mean and covariance matrix $\mathbf{Q}=E[\mathbf{e}_k\mathbf{e}_k^{\mathrm{T}}]$. Note that $\mathbf{e}_k$ is uncorrelated to $\mathbf{y}_{k-1}^{-}$ and hence to $\mathbf{z}_k$ by construction, and that the elements of $\mathbf{e}_k$ are serially uncorrelated. $\mathbf{z}_k$ is an $(n\times 1)$ vector of unobservable states that are minimal sufficient statistics (optimal carriers of information) for the history of the process $\mathbf{y}_k$. The $(n\times m)$ matrix $\mathbf{B}$ is called the Kalman gain [8,11]. Since

$$\mathbf{x}_{k+1}=E[\mathbf{x}_{k+1}|\mathbf{e}_k^{\mathrm{T}}](E[\mathbf{e}_k\mathbf{e}_k^{\mathrm{T}}])^{-1}\mathbf{e}_k \tag{51}$$

the following relation is obtained:

$$\mathbf{B}=E[\mathbf{x}_{k+1}\mathbf{e}_k^{\mathrm{T}}](E[\mathbf{e}_k\mathbf{e}_k^{\mathrm{T}}])^{-1}. \tag{52}$$

Note that by assumption $\mathbf{u}_k|\mathbf{y}_{k-1}^{-}=0$ and $\mathbf{v}_k|\mathbf{y}_{k-1}^{-}=0$. Using the definition of $\mathbf{e}_k$ and Eq. (37), the discrete time observation equation which contains the innovation vector is obtained

$$\mathbf{y}_k=(\mathbf{C}\mathbf{x}_k+\mathbf{v}_k)|\mathbf{y}_{k-1}^{-}+\mathbf{e}_k=\mathbf{C}(\mathbf{x}_k|\mathbf{y}_{k-1}^{-})+\mathbf{e}_k=\mathbf{C}\mathbf{z}_k+\mathbf{e}_k. \tag{53}$$

The set of Eqs. (36) and (37) is now replaced by

$$\mathbf{z}_{k+1}=\mathbf{A}\mathbf{z}_k+\mathbf{B}\mathbf{e}_k \tag{54}$$

$$\mathbf{y}_k = \mathbf{C}\mathbf{z}_k + \mathbf{e}_k. \tag{55}$$

Such a representation is called an innovation representation of the data-generating process (36) and (37). The aim of the mutual information method consists in the optimization of the mutual information between future observations $\mathbf{y}_k^+$ and the state $\mathbf{z}_k$ which is expressed as a linear transformation of the past: $\mathbf{z}_k = \mathbf{S}\mathbf{y}_{k-1}^-$ [11]. Let $I(\mathbf{y}_k^+, \mathbf{z}_k)$ be the mutual information between $\mathbf{y}_k^+$ and $\mathbf{z}_k$ defined as follows:

$$I(\mathbf{y}_k^+, \mathbf{z}_k) = \Pi(\mathbf{y}_k^+) + \Pi(\mathbf{z}_k) - \Pi(\mathbf{y}_k^+/\mathbf{z}_k) \tag{56}$$

where $\Pi(\mathbf{y}_k^+)$ is the entropy of $\mathbf{y}_k^+$, $\Pi(\mathbf{z}_k)$ the entropy of $\mathbf{z}_k$ and $\Pi(\mathbf{y}_k^+/\mathbf{z}_k)$ the conditional entropy. The following maximization problem is defined:

$$\begin{cases} \text{Max } I(\mathbf{y}_k^+, \mathbf{z}_k) \\ \mathbf{z}_k. \end{cases} \tag{57}$$

Since $\mathbf{z}_k = \mathbf{S}\mathbf{y}_{k-1}^-$, the problem is to find the $(n \times mp)$ matrix $\mathbf{S}$ which maximizes $I(\mathbf{y}_k^+, \mathbf{S}\mathbf{y}_{k-1}^-)$. Using the properties of gaussian vectors ($\mathbf{y}_k^+$ and $\mathbf{y}_{k-1}^-$ are gaussian) the following relation is obtained:

$$\Pi(\mathbf{y}_k^+) = \ln(\det(\mathbf{R}_+)) \quad \Pi(\mathbf{S}\mathbf{y}_{k-1}^-) = \ln(\det(\mathbf{S}\mathbf{R}_-\mathbf{S}^{\mathrm{T}})) \tag{58}$$

$$\Pi(\mathbf{y}_k^+/\mathbf{S}_{k+1}^-) = \ln\left(\det\left(\begin{bmatrix} \mathbf{R}_+ & \mathbf{H}\mathbf{S}^{\mathrm{T}} \\ \mathbf{S}\mathbf{H}^{\mathrm{T}} & \mathbf{S}\mathbf{R}_-\mathbf{S}^{\mathrm{T}} \end{bmatrix}\right)\right) \tag{59}$$

where $\mathbf{R}_+ = E[\mathbf{y}_k^+(\mathbf{y}_k^+)^{\mathrm{T}}]$ and $\mathbf{R}_- = E[\mathbf{y}_{k-1}^-(\mathbf{y}_{k-1}^-)^{\mathrm{T}}]$.

Using the fact that

$$\det\begin{bmatrix} \mathbf{R}_+ & \mathbf{H}\mathbf{S}^{\mathrm{T}} \\ \mathbf{S}\mathbf{H}^{\mathrm{T}} & \mathbf{S}\mathbf{R}_-\mathbf{S}^{\mathrm{T}} \end{bmatrix} = \det(\mathbf{S}\mathbf{R}_-\mathbf{S}^{\mathrm{T}}) \times \det(\mathbf{R}_+ - \mathbf{H}\mathbf{S}^{\mathrm{T}}(\mathbf{S}\mathbf{R}_-\mathbf{S}^{\mathrm{T}})^{-1}\mathbf{S}\mathbf{H}^{\mathrm{T}}) \tag{60}$$

the following formula is obtained:

$$\Pi(\mathbf{y}_k^+/\mathbf{S}\mathbf{y}_k^-) = \ln(\det(\mathbf{S}\mathbf{R}_-\mathbf{S}^{\mathrm{T}})) + \ln(\det(\mathbf{R}_+ - \mathbf{H}\mathbf{S}^{\mathrm{T}}(\mathbf{S}\mathbf{R}_-\mathbf{S}^{\mathrm{T}})^{-1}\mathbf{S}\mathbf{H}^{\mathrm{T}})). \tag{61}$$

The estimation of $\mathbf{S}$ amounts to minimizing the following criterion:

$$\begin{cases} \text{Min } \det(\mathbf{R}_+ - \mathbf{H}\mathbf{S}^{\mathrm{T}}(\mathbf{S}\mathbf{R}_-\mathbf{S}^{\mathrm{T}})^{-1}\mathbf{S}\mathbf{H}^{\mathrm{T}}) \\ \mathbf{S}(n \times mp). \end{cases} \tag{62}$$

The estimate of $\mathbf{S}$ is obtained from

$$\begin{cases} \text{Min } \det(\mathbf{I}_{mf} - \mathbf{R}_+^{-1/2} - \mathbf{H}\mathbf{S}^{\mathrm{T}}(\mathbf{S}\mathbf{R}_-\mathbf{S}^{\mathrm{T}})^{-1}\mathbf{S}\mathbf{H}^{\mathrm{T}}\mathbf{R}_+^{-1/2}) \\ \mathbf{S}(n \times mp) \end{cases} \tag{63}$$

$$\begin{cases} \text{Min } \prod_{i=1}^{n}(1-\mu_i) \\ \mathbf{S}(n \times mp) \end{cases} \tag{64}$$

where μ_i are the non-zero eigenvalues of $\mathbf{\Omega} = \mathbf{R}_+^{-1/2}\mathbf{H}\mathbf{S}^{\mathrm{T}}(\mathbf{S}\mathbf{R} - \mathbf{S}^{\mathrm{T}})^{-1}\mathbf{S}\mathbf{H}^{\mathrm{T}}\mathbf{R}_+^{-1/2}$. Change the variable as $\mathbf{S} = \mathbf{Z}\mathbf{E}^{\mathrm{T}}\mathbf{R}_-^{-1/2}$ where $\mathbf{Z}$ is an $(n \times n)$ matrix of full rank and $\mathbf{E}$ is an $(mp \times n)$ orthogonal matrix to determine. The matrix $\mathbf{\Omega}$ is then given by

$$\mathbf{\Omega} = \mathbf{R}_+^{-1/2}\mathbf{H}\mathbf{R}_-^{-1/2}\mathbf{E}\mathbf{E}^{\mathrm{T}}\mathbf{R}_-^{-1/2}\mathbf{H}^{\mathrm{T}}\mathbf{R}_+^{-1/2}. \tag{65}$$

The eigenvalues of $\mathbf{\Omega}$ are

$$\lambda(\mathbf{\Omega}) = \lambda(\mathbf{R}_+^{-1/2}\mathbf{H}\mathbf{R}_-^{-1/2}\mathbf{E}\mathbf{E}^{\mathrm{T}}\mathbf{R}_-^{-1/2}\mathbf{H}^{\mathrm{T}}\mathbf{R}_+^{-1/2}). \tag{66}$$

Since $\lambda(ab) = \lambda(ba)$, the eigenvalue of $\mathbf{\Omega}$ are given by $\lambda[\mathbf{E}^{\mathrm{T}}(\mathbf{R}_+^{-1/2}\mathbf{H}\mathbf{R}_-^{-1/2})^{\mathrm{T}}(\mathbf{R}_+^{-1/2}\mathbf{H}\mathbf{R}_-^{-1/2})\mathbf{E}]$ and are bounded by the n largest eigenvalues of $(\mathbf{R}_+^{-1/2}\mathbf{H}\mathbf{R}_-^{-1/2})^{\mathrm{T}}(\mathbf{R}_+^{-1/2}\mathbf{H}\mathbf{R}_-^{-1/2})$.

The bound is attained if $\mathbf{E}$ is taken as the eigenvector corresponding to the n largest eigenvalues of $(\mathbf{R}_+^{-1/2}\mathbf{H}\mathbf{R}_-^{-1/2})^{\mathrm{T}}(\mathbf{R}_+^{-1/2}\mathbf{H}\mathbf{R}_-^{-1/2})$. Introduce the singular value decomposition of $\mathbf{R}_+^{-1/2}\mathbf{H}\mathbf{R}_-^{-1/2}$

$$\mathbf{R}_+^{-1/2}\mathbf{H}\mathbf{R}_-^{-1/2} = \mathbf{U}\boldsymbol{\Sigma}\mathbf{V}^{\mathrm{T}} = [\mathbf{U}_n \ \ \mathbf{U}_0]\begin{bmatrix}\boldsymbol{\Sigma}_n & 0\\ 0 & \boldsymbol{\Sigma}_0\end{bmatrix}\begin{bmatrix}\mathbf{V}_n^{\mathrm{T}}\\ \mathbf{V}_0^{\mathrm{T}}\end{bmatrix} \tag{67}$$

where $\mathbf{U}_n$ and $\mathbf{V}_n$ are $(mf \times n)$ and $(mp \times n)$ matrices containing the first n left and right singular vectors. They verify $\mathbf{U}_n^{\mathrm{T}}\mathbf{U}_n = \mathbf{I}_n$ and $\mathbf{V}_n^{\mathrm{T}}\mathbf{V}_n = \mathbf{I}_n$ and Σ_n is the $(n \times n)$ diagonal matrix containing the first n singular values.

The eigenvalue decomposition of $(\mathbf{R}_+^{-1/2}\mathbf{H}\mathbf{R}_-^{-1/2})^{\mathrm{T}}(\mathbf{R}_+^{-1/2}\mathbf{H}\mathbf{R}_-^{-1/2})$ is then given by $\mathbf{V}\boldsymbol{\Sigma}^2\mathbf{V}^{\mathrm{T}}$ and the upper bound on the eigenvalues of $\boldsymbol{\Omega}$ is attained if $\mathbf{E} = \mathbf{V}_n$. The solution of our minimization problem (64) is given by $\mathbf{S} = \mathbf{Z}\mathbf{V}_n^{\mathrm{T}}\mathbf{R}_-^{-1/2}$ and the state $\mathbf{z}_k$ takes the form

$$\mathbf{z}_k = \mathbf{Z}\mathbf{V}_n^{\mathrm{T}}\mathbf{R}_-^{-1/2}\mathbf{y}_{k-1}^-. \tag{68}$$

To estimate the parameters of the state-space model the definition of orthogonal projection of random variables is used. To obtain a relation for $\mathbf{A}$, we observe that

$$\mathbf{z}_{k+1}|\mathbf{z}_k = E[\mathbf{z}_{k+1}\mathbf{z}_k^{\mathrm{T}}](E[\mathbf{z}_k\mathbf{z}_k^{\mathrm{T}}])^{-1} = \mathbf{A}\mathbf{z}_k. \tag{69}$$

Then

$$\mathbf{A} = E[\mathbf{z}_{k+1}\mathbf{z}_k^{\mathrm{T}}](E[\mathbf{z}_k\mathbf{z}_k^{\mathrm{T}}])^{-1} = \mathbf{S}E[\mathbf{y}_{k-1}^-(\mathbf{y}_{k-1}^-)^{\mathrm{T}}]\mathbf{S}^{\mathrm{T}}(\mathbf{S}E[\mathbf{y}_{k-1}^-(\mathbf{y}_{k-1}^-)^{\mathrm{T}}]\mathbf{S}^{\mathrm{T}})^{-1}. \tag{70}$$

It is useful to define the block $(mp \times mp)$ covariance matrix $\mathbf{R}_- = E[\mathbf{y}_{k-1}^-(\mathbf{y}_{k-1}^-)^{\mathrm{T}}]$ and its left-shifted variant $\mathbf{R}_-^{\leftarrow} = E[\mathbf{y}_k^-(\mathbf{y}_{k-1}^-)^{\mathrm{T}}]$ to obtain

$$\mathbf{A} = \mathbf{S}\mathbf{R}_-^{\leftarrow}\mathbf{S}^{\mathrm{T}}(\mathbf{S}\mathbf{R}_-\mathbf{S}^{\mathrm{T}})^{-1} = (\mathbf{Z}^{\mathrm{T}}\mathbf{V}_n^{\mathrm{T}}\mathbf{R}_-^{-1/2}\mathbf{R}_-^{\leftarrow}\mathbf{R}_-^{-1/2}\mathbf{V}_n\mathbf{Z})(\mathbf{Z}^{\mathrm{T}}\mathbf{Z})^{-1}. \tag{71}$$

To obtain a relation for $\mathbf{C}$, the orthogonal projection between the data $\mathbf{y}_k$ and the states $\mathbf{z}_k$ is considered

$$\mathbf{y}_k|\mathbf{z}_k = E[\mathbf{y}_k\mathbf{z}_k^{\mathrm{T}}](E[\mathbf{z}_k\mathbf{z}_k^{\mathrm{T}}])^{-1}\mathbf{z}_k = \mathbf{C}\mathbf{z}_k \tag{72}$$

$$\mathbf{C} = E[\mathbf{y}_k\mathbf{z}_k^{\mathrm{T}}](E[\mathbf{z}_k\mathbf{z}_k^{\mathrm{T}}])^{-1} = E[\mathbf{y}_k(\mathbf{y}_{k-1}^-)^{\mathrm{T}}]\mathbf{S}^{\mathrm{T}}(\mathbf{S}E[\mathbf{y}_{k-1}^-(\mathbf{y}_{k-1}^-)^{\mathrm{T}}]\mathbf{S}^{\mathrm{T}})^{-1} \tag{73}$$

$$\mathbf{C} = [\mathbf{R}_1 \ \ \mathbf{R}_2 \ \ \cdots \ \ \mathbf{R}_p]\mathbf{S}^{\mathrm{T}}(\mathbf{S}\mathbf{R}_-\mathbf{S}^{\mathrm{T}})^{-1} = [\mathbf{R}_1 \ \ \mathbf{R}_2 \ \ \cdots \ \ \mathbf{R}_p]\mathbf{R}_-^{-1/2}\mathbf{V}_n\mathbf{Z}(\mathbf{Z}^{\mathrm{T}}\mathbf{Z})^{-1}. \tag{74}$$

In the paper we consider $\mathbf{Z} = \mathbf{I}_n$. Knowing the transition matrix $\mathbf{A}$ and the output influence matrix $\mathbf{C}$, it is possible to identify the eigenfrequencies, damping ratios and mode shapes of mistuned bladed disks from

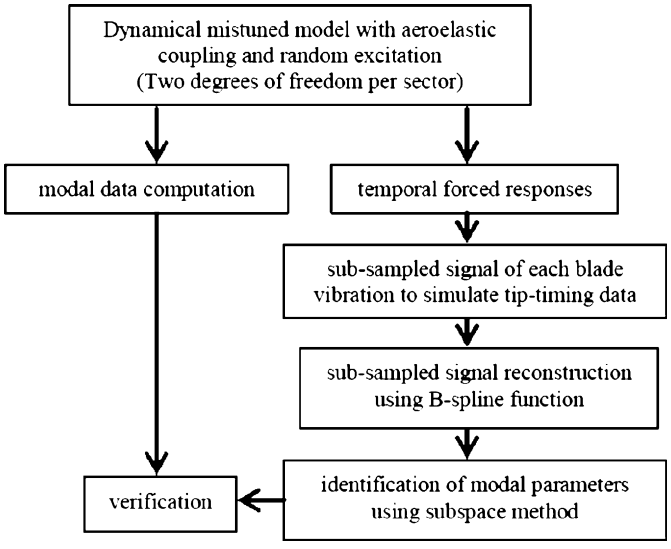

Fig. 7. Methodology used in this paper.

reconstructed tip timing signals. The comparison of the shifted observability matrix method and the mutual information criterion method in modal parameter identification is presented in the next section. Fig. 7 summarizes the identification procedure used in the paper.

8. Analysis of identification results

The subspace modal identification algorithms developed have been applied to time responses of 28 min and 24 s, generated from the mechanical model presented previously. The sampling period is $\Delta t = 7 \cdot 10^{-3}$ s. Two approaches can be used in the identification process: a local and a global approach. The local approach uses the temporal response of each blade alone. The global approach uses all temporal blade responses. In this paper a global approach is used; this approach allows the mode shape identification of bladed assemblies. The stability diagram involves tracking the estimates of eigenfrequencies and damping ratios as a function of model order. As the model order is increased, more and more modal frequencies and damping ratios are

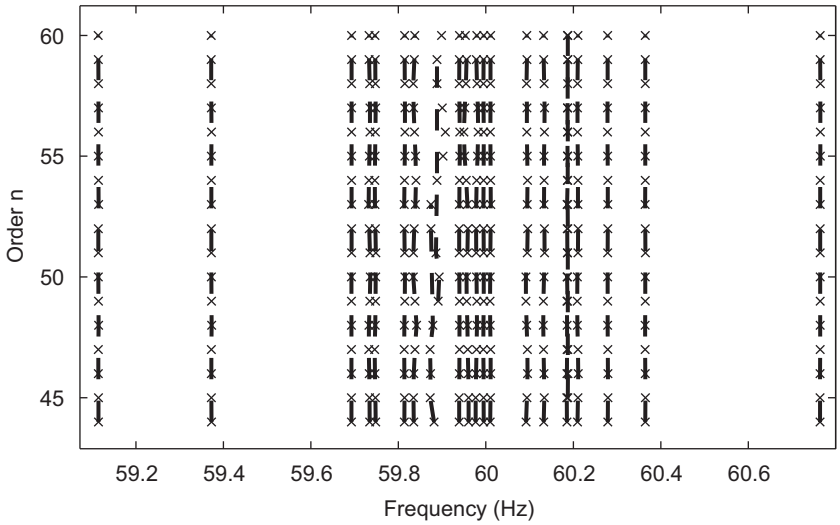

Fig. 8. Stability diagram on eigenfrequencies using the shifted observability matrix method.

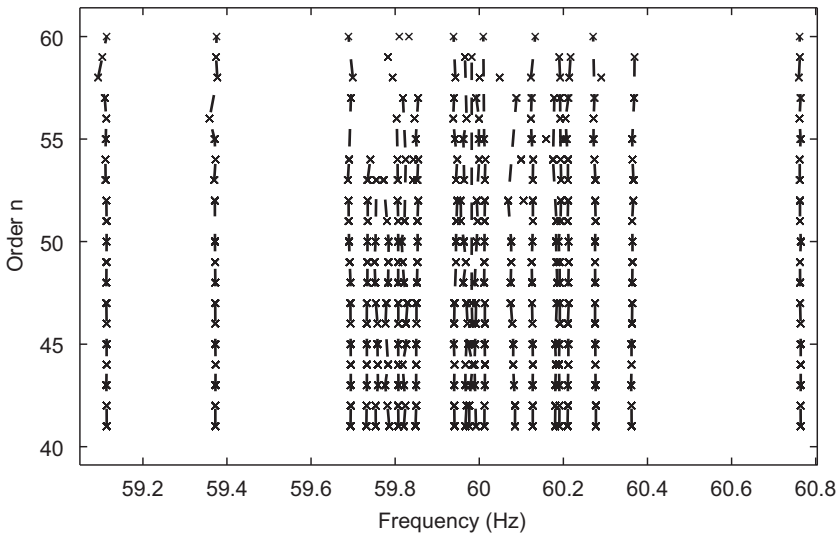

Fig. 9. Stability diagram on eigenfrequencies using the mutual information criterion method.

estimated; hopefully, the estimates of the physical modal parameters stabilize as the correct model order is reached. For modes which are very active in the measured data, the modal parameters stabilize at a very low model order. For modes poorly excited, the modal parameters may not stabilize until a very high model order is chosen. Nevertheless, the non-physical modes, essentially computational modes, do not stabilize at all during this process and can be sorted out of the modal parameters. Figs. 8 and 9 show the stability diagrams on eigenfrequencies using the shifted observability matrix method and the mutual information criterion

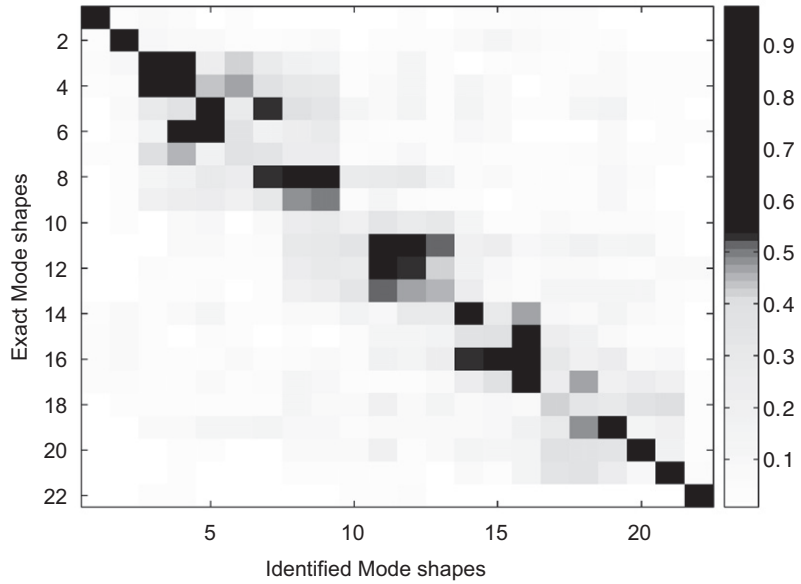

Fig. 10. Comparison of mode shapes using the MAC with the observability matrix method.

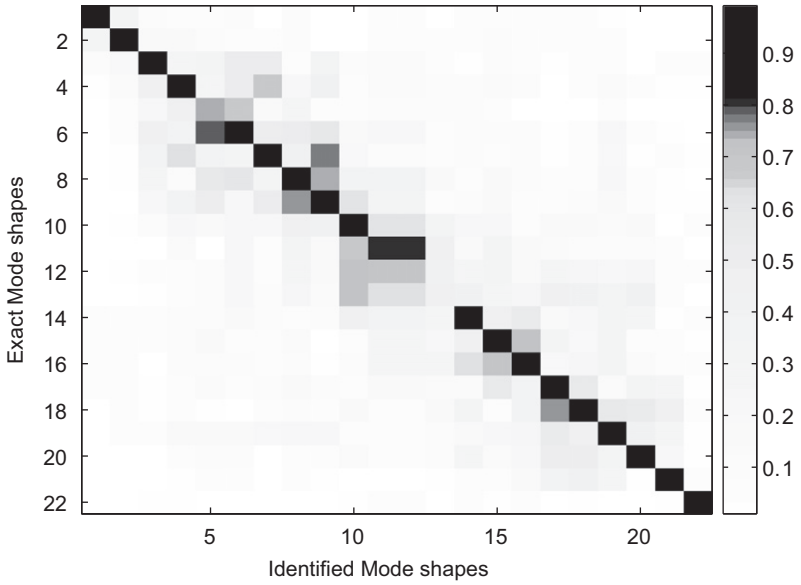

Fig. 11. Comparison of mode shapes using the MAC with the mutual information method.

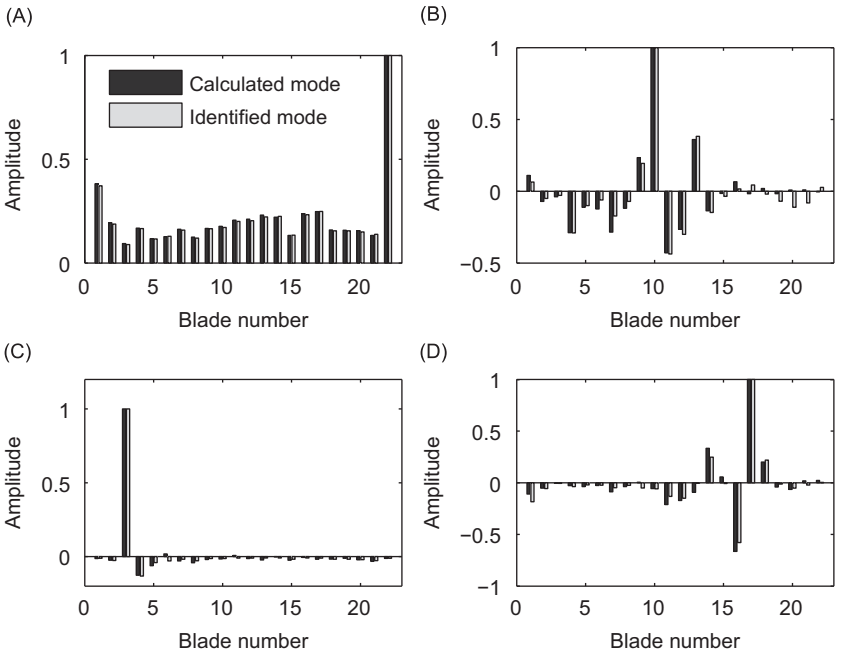

Fig. 12. Comparison between identified and exact mode shapes: (A) mode shape number 1; (B) mode shape number 10; (C) mode shape number 22; (D) mode shape number 5.

Table 1
Comparison between exact and identified results (shifted observability method)

	Comparison between exact and identified results					
	Identified results		Exact results		Error on frequency (%)	Error on damping ratio (%)
	Frequency (Hz)	Damping ratio (%)	Frequency (Hz)	Damping ratio (%)		
Mode no. 1	59.11	0.096	59.11	0.095	0.00	1.05
Mode no. 2	59.37	0.137	59.37	0.138	0.00	0.72
Mode no. 3	59.69	0.169	59.69	0.168	0.00	0.6
Mode no. 4	59.73	0.175	59.73	0.159	0.00	10.1
Mode no. 5	59.74	0.270	59.74	0.296	0.00	8.8
Mode no. 6	59.81	0.199	59.77	0.248	0.07	60
Mode no. 7	59.84	0.100	59.81	0.092	0.05	116
Mode no. 8	59.88	0.352	59.83	0.272	0.08	29
Mode no. 9	59.89	0.367	59.86	0.172	0.05	113
Mode no. 10	59.94	0.174	59.93	0.162	0.02	7.4
Mode no. 11	59.96	0.262	59.96	0.269	0.00	2.6
Mode no. 12	59.98	0.242	59.97	0.221	0.02	9.5
Mode no. 13	59.99	0.184	59.99	0.181	0.00	1.66
Mode no. 14	60.01	0.137	60.00	0.127	0.02	7.87
Mode no. 15	60.09	0.320	60.10	0.294	0.02	8.8
Mode no. 16	60.13	0.174	60.13	0.156	0.00	11.5
Mode no. 17	60.19	0.233	60.18	0.251	0.02	7.2
Mode no. 18	60.19	0.222	60.19	0.212	0.00	4.7
Mode no. 19	60.21	0.222	60.20	0.209	0.02	6.2
Mode no. 20	60.28	0.198	60.28	0.211	0.00	6.2
Mode no. 21	60.36	0.231	60.36	0.228	0.00	1.32
Mode no. 22	60.76	0.227	60.77	0.207	0.02	9.7

method. From these plots we can identify easily the eigenfrequencies of 22 blades. We can see that all eigenfrequencies are stable.

The exact mode shapes can be compared with the identified mode shapes using the modal assurance criterion (MAC): let $\mathbf{\Phi}_i$ be the ith exact mode shape and $\tilde{\mathbf{\Phi}}_j$ the jth identified mode shape; the MAC matrix is defined as

$$\mathbf{MAC}_{ij} = \frac{|\mathbf{\Phi}_i^* \tilde{\mathbf{\Phi}}_j|}{\sqrt{(\mathbf{\Phi}_i^* \mathbf{\Phi}_i)(\tilde{\mathbf{\Phi}}_j^* \tilde{\mathbf{\Phi}}_j)}} \tag{75}$$

where $(.)^*$ is the complex conjugate transpose.

The MAC indicates the degree of correlation between the mode shapes. For two vectors that are proportional the MAC equals 1 (perfect correlation) and values above 0.8 are highly correlated. Values below 0.6 should be considered with much caution: the correlation is not well defined. Fig. 10 shows the values of the MAC matrix for the 22 blades, using the shifted observability matrix method. From this figure we can see that eight modes, 6, 7, 9, 10, 13, 15, 17 and 18, have not been found by the identification process using the shifted observability matrix method. The values of the MAC are lower than 0.6 for these eight modes. For the remaining modes the correlation between exact and identified modes is acceptable or even excellent. Fig. 11 shows the values of the MAC matrix using the mutual information criterion method. From this figure we observe that only one mode, the mode number 13, is not identified by this method. Fig. 12 shows a comparison between some exact and identified mode shapes. The identified mode shapes can be compared to the exact ones in the following manner: for each complex mode $\mathbf{\Phi}$, we define a real mode $\mathbf{\Phi}_R$ as the deflection for the instant of time where the maximum amplitude is obtained. Four of these modes are shown in Fig. 12. These results are obtained using the mutual information criterion method.

Table 2
Comparison between exact and identified results (mutual information method)

	Comparison between exact and identified results					
	Identified results		Exact results		Error on frequency (%)	Error on damping ratio (%)
	Frequency (Hz)	Damping ratio (%)	Frequency (Hz)	Damping ratio (%)		
Mode no. 1	59.11	0.098	59.11	0.095	0.00	3.16
Mode no. 2	59.37	0.141	59.38	0.137	0.02	2.92
Mode no. 3	59.69	0.160	59.70	0.168	0.02	4.76
Mode no. 4	59.73	0.158	59.73	0.159	0.00	0.63
Mode no. 5	59.76	0.289	59.75	0.295	0.02	2
Mode no. 6	59.78	0.258	59.78	0.248	0.00	4
Mode no. 7	59.81	0.097	59.81	0.093	0.00	4.3
Mode no. 8	59.82	0.330	59.83	0.272	0.02	21
Mode no. 9	59.85	0.159	59.86	0.172	0.02	7.56
Mode no. 10	59.94	0.167	59.93	0.161	0.02	3.73
Mode no. 11	59.97	0.237	59.96	0.269	0.02	12
Mode no. 12	59.98	0.272	59.97	0.221	0.02	23
Mode no. 13	59.99	0.187	59.99	0.181	0.00	3.31
Mode no. 14	60.01	0.134	60.01	0.127	0.00	5.51
Mode no. 15	60.08	0.282	60.10	0.294	0.03	4.1
Mode no. 16	60.13	0.159	60.13	0.156	0.00	1.92
Mode no. 17	60.18	0.247	60.18	0.251	0.00	1.59
Mode no. 18	60.19	0.212	60.19	0.212	0.00	0.00
Mode no. 19	60.21	0.223	60.20	0.209	0.02	6.70
Mode no. 20	60.28	0.194	60.28	0.211	0.00	8.1
Mode no. 21	60.36	0.231	60.36	0.228	0.00	1.32
Mode no. 22	60.76	0.235	60.77	0.207	0.02	14

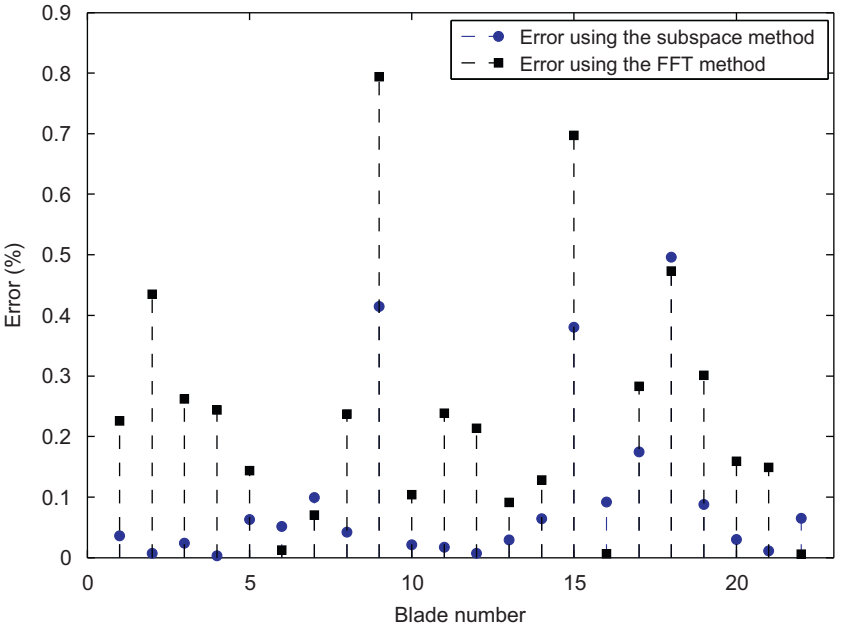

Fig. 13. Comparison between frequency identification errors.

Table 1 shows the exact and identified values on eigenfrequencies and damping ratios using the shifted observability matrix method. The relative errors between the exact and the identified eigenfrequencies are lower than 0.08% and the relative errors on damping ratios are higher than 10% for six modes, the maximal value being 116% for the seventh mode. Table 2 shows the exact and identified values on eigenfrequencies and damping ratios using the mutual information criterion method. The relative errors between the exact and the identified eigenfrequencies are lower than 0.02% and the relative errors on damping ratios are higher than 10% for four modes, the maximal value being 23% for the twelfth mode.

The discrete-time data sequence $\{y_k\}$ possesses a discrete-time Fourier transform and from this transform we find the frequency component of this signal, plotting the power spectral density which is a measurement of the energy at various frequencies. The peaks of resonance of a blade appear when we plot the power spectral density. However, often spurious or artefact peaks appear in these plots and it is very difficult to differentiate spurious frequencies and true eigenfrequencies of blades. This technique is called the standard FFT method. Fig. 13 shows the error in percent between the exact and the identified eigenfrequencies using the standard FFT method and the mutual information criterion method proposed in the paper. We have applied the FFT and the subspace algorithm to each blade alone: a local approach has been used in this example. From this figure we can conclude that the subspace method works better than the traditional FFT method. We also note that the global approach gives better results than the local approach. There are at least two reasons for the use of the subspace method instead of the traditional FFT method:

- the subspace method gives a smaller error on identified eigenfrequencies than the FFT method as shown in Fig. 13;
- if we use the FFT method we cannot obtain the damping coefficients of blades. Using the subspace method and in particular the mutual information criterion, the damping coefficients can be identified.

9. Conclusion

The determination of the vibration characteristics of rotating engine blades is very important for fatigue failure considerations. One of the most promising techniques for measuring the modal parameters of blade

vibrations is blade tip timing. Tip timing data are generated using mistuned models which are obtained by adding stiffness variations to nominal blade stiffness. Two identification procedures based on subspace methods are compared using data obtained from a reconstruction signal. The first subspace method uses properties of the observability matrix to obtain the transition matrix which contains all modal information about the vibrating system. The second method uses the mutual information between the future data vector of observations and the state vector. The transition matrix is computed again. These two methods are a real improvement to the traditional FFT method. Using subspace methods, and in particular the mutual information criterion, the damping ratios and the mode shapes can be identified with reasonable error. Note that the two subspace methods give good results in the identification of closely spaced eigenfrequencies. In the future we shall study the effect of signal to noise ratio on the identification of modal parameters. The reconstruction of temporal signals from identified modal parameters and the identification of aeroelastic coupling and aerodynamic excitation are also under investigation.

Acknowledgements

The authors would like to thank EDF R& D who supported this work.

Appendix A

The form of the aeroelastic matrix is

$$\mathbf{C}_{\text{aero}} = \begin{bmatrix} C_0 & 0 & C_1 & 0 & C_2 & 0 & \cdots & \cdots & 0 & C_{-2} & 0 & C_{-1} \\ 0 & 0 & \cdots & & & & & & & & & 0 \\ C_{-1} & 0 & C_0 & 0 & C_1 & 0 & C_2 & 0 & 0 & \cdots & 0 & C_{-2} \\ 0 & 0 & \cdots & & & & & & & & & 0 \\ C_{-2} & 0 & C_{-1} & 0 & C_0 & 0 & C_1 & 0 & C_2 & 0 & \cdots & 0 \\ 0 & 0 & \cdots & & & & & & & & & 0 \\ 0 & 0 & C_{-2} & 0 & C_{-1} & 0 & C_0 & 0 & C_1 & 0 & C_2 & \cdot \\ \vdots & \vdots & \vdots & \vdots & \vdots & \vdots & \vdots & \vdots & \vdots & \vdots & \vdots & \vdots \\ C_2 & 0 & \cdots & 0 & C_{-2} & 0 & C_{-1} & 0 & C_0 & 0 & C_1 & \\ 0 & 0 & \cdots & & & & & & & & & 0 \\ C_1 & 0 & C_2 & 0 & 0 & \cdots & 0 & C_{-2} & 0 & C_{-1} & 0 & C_0 \end{bmatrix}. \tag{76}$$

The value 0 between the aeroelastic coefficients represents the excitation on the dof corresponding to the disk. The coefficients C_k are given by the following relation:

$$C_k = |C_k| e^{j(\Phi_k + \omega t)}$$

and $\mathbf{F}_{\text{aero}}(t)$ can be written as

$$\mathbf{F}_{\text{aero}}(t) = |C_k| e^{j(\Phi_k + \omega t)} \dot{\mathbf{Q}}$$

where $\dot{\mathbf{Q}}$ is the real part of the velocity amplitude, and $|C_k|$ and Φ_k are the amplitude and phase of the aeroelastic coefficients. These two values are given by our industrial partner using a finite element model.

We then obtain

$$\mathbf{F}_{\text{aero}}(t) = |C_k|(\dot{\mathbf{q}}(t)\cos(\phi_k) - \omega \mathbf{q}(t)\sin(\Phi_k)) = \mathbf{C}^R_{\text{aero}}\dot{\mathbf{q}}(t) - \omega \mathbf{C}^I_{\text{aero}}\mathbf{q}(t).$$

The two matrices $\mathbf{C}^I_{\text{aero}}$ and $\mathbf{C}^R_{\text{aero}}$ have the same form as $\mathbf{C}_{\text{aero}}$ and are given by the following relations:

$$\mathbf{C}^I_{\text{aero}} = |C_k| \sin(\Phi_k)$$

and

$$\mathbf{C}^{R}_{\text{aero}} = |C_k| \cos(\Phi_k).$$

Appendix B

The eigenvalues λ_i of the transition matrix $\mathbf{A}$ are:

$$\lambda_i = \mathrm{e}^{\mu_i \Delta t}$$

where $i = 1, 2, \ldots, n$. This relation is rewritten in the following way:

$$\lambda_i = \mathrm{e}^{-\xi_i \omega_i + j\omega_i \sqrt{(1-\xi_i^2)}\Delta t}$$

$$\lambda_i^* = \mathrm{e}^{-\xi_i \omega_i - j\omega_i \sqrt{(1-\xi_i^2)}\Delta t}$$

$$\lambda_i + \lambda_i^* = 2\mathrm{e}^{-\xi_i \omega_i \Delta t} \cos(\omega_i \sqrt{(1-\xi_i^2)}\Delta t)$$

$$\lambda_i \lambda_i^* = \mathrm{e}^{-2\xi_i \omega_i \Delta t}$$

$$\omega_i \sqrt{(1-\xi_i^2)} = \frac{1}{\Delta t} \arccos\left(\frac{\lambda_i + \lambda_i^*}{2\sqrt{\lambda_i \lambda_i^*}}\right)$$

$$\ln \lambda_i \lambda_i^* = -2\xi_i \omega_i \Delta t$$

$$\omega_i^2 = \frac{1}{(1-\xi_i^2)\Delta t^2} \left[\arccos\left(\frac{\lambda_i + \lambda_i^*}{2\sqrt{\lambda_i \lambda_i^*}}\right)\right]^2$$

and

$$\xi_i^2 \omega_i^2 = \frac{[\ln(\lambda_i \lambda_i^*)]^2}{4\Delta t^2}$$

$$\frac{1-\xi_i^2}{\xi_i^2} = \frac{1}{\xi_i^2} - 1 = \frac{4}{[\ln(\lambda_i \lambda_i^*)]^2} \left[\arccos\left(\frac{\lambda_i + \lambda_i^*}{2\sqrt{\lambda_i \lambda_i^*}}\right)\right]^2.$$

We then obtain the damping coefficients and the eigenfrequencies using

$$\xi_i = \sqrt{\frac{[\ln(\lambda_i \lambda_i^*)]^2}{[\ln(\lambda_i \lambda_i^*)]^2 + 4\left[\arccos\left(\frac{\lambda_i + \lambda_i^*}{2\sqrt{\lambda_i \lambda_i^*}}\right)\right]^2}}$$

$$f_i = \sqrt{\frac{1}{2\pi\Delta t}\left\{[\ln(\lambda_i \lambda_i^*)]^2 + 4\left[\arccos\left(\frac{\lambda_i + \lambda_i^*}{2\sqrt{\lambda_i \lambda_i^*}}\right)\right]^2\right\}}.$$

References

[1] I.B. Carrington, J.R. Wright, J.E. Cooper, G. Dimitriadis, A comparison of blade tip timing data analysis methods, *Proceedings of the Institution of Mechanical Engineers* 215 (G) (2001) 301–312.

[2] G. Dimitriadis, B. Carrington, J.R. Wright, J.E. Cooper, Blade tip timing measurement of synchronous vibrations of rotating bladed assemblies, *Mechanical Systems and Signal Processing* 16 (4) (2002) 599–622.
[3] C.P. Lawson, P.C. Ivey, Turbo-machinery blade vibration amplitude measurement through tip timing with capacitance tip clearance probes, *Sensors and Actuators A* 118 (2005) 14–24.
[4] S. Heath, A new technique for identifying synchronous resonances using tip timing, *Journal of Engineering for Gas Turbines and Power* 122 (2000) 219–225.
[5] P.C. Ivey, K.R. Grant, C. Lawson, *Tip timing techniques for turbomachinery HCF condition monitoring, The 16th Symposium on Measuring Techniques in Transonic and Supersonic Flow*, Cambridge, UK, 2002.
[6] E.F. Crawley, Aeroelastic formulation for tuned and mistuned rotors, AGARD Manual on Aeroelasticity in Axial-Flow Turbomachines, Vol. 19, 1988.
[7] S. Ries, Digital time-delay beamforming with interpolated signals, *Signal Processing* 84 (2004) 2403–2423.
[8] J.N. Juang, *Applied System Identification*, Prentice-Hall, Englewood Cliffs, NJ, 1994.
[9] J. Lardiès, On the use of Padé approximants in the estimation of eigenfrequencies and damping ratios of a vibrating system, *Journal of Sound and Vibration* 292 (2006) 571–582.
[10] J. Lardiès, A stochastic realisation algorithm with application to modal parameter estimation, *Mechanical Systems and Signal Processing* 15 (2) (1998) 275–285.
[11] M. Aoki, *State Space Modeling of Time Series*, second ed., Springer, Berlin, 1990.
[12] G.H. Golub, C. Van Loan, *Matrix Computations*, third ed., Johns Hopkins University Press, Baltimore, M.D., 1996.